Venegas, M., de Vega, M., García-Hernando, N. & Ruiz-Rivas, U. (2017). Adiabatic vs non-adiabatic membrane-based rectangular micro-absorbers for H2O-LiBr absorption chillers. *Energy*, vol. 134, pp. 757–766.

DOI: 10.1016/j.energy.2017.06.068

Adiabatic vs non-adiabatic membrane-based rectangular micro-absorbers for H_2O-LiBr absorption chillers

M. Venegas [a,b,c*], M. de Vega [a,c], N. García-Hernando [a,c], U. Ruiz-Rivas [a,b]

[a] ISE Research Group, Department of Thermal and Fluids Engineering, Universidad Carlos III de Madrid, Avda. Universidad 30, 28911 Leganés, Madrid, Spain
[b] GTADS Research Group, Department of Thermal and Fluids Engineering, Universidad Carlos III de Madrid, Avda. Universidad 30, 28911 Leganés, Madrid, Spain
[c] Associated Research Unit CSIC-Universidad Carlos III de Madrid, Spain

Abstract

In this paper a microporous membrane is used in combination with rectangular microchannels in the absorber of an absorption chiller, working in two different configurations: cooled by a water flow and adiabatically. In the non-adiabatic case, the configuration of the channels allows the heat released during absorption to be extracted using a cooling water flow. The results for solution concentration, pressure potential, absorption coefficient, absorption rate, temperatures and power exchanged/stored by the working fluids along the absorption channels are presented. The ratio between the cooling power of the chiller equipped with the simulated absorber and the absorber volume, r_{qV}, is used to characterise the absorber compactness. A parametric analysis is also performed to evaluate the influence on the ratio r_{qV} of the inlet solution mass flow rate, the solution inlet temperature, and the height and width of the solution channels, for both absorbers. For the base case considered in this study, both absorber configurations offer r_{qV} higher than 1 MW m^{-3}. This ratio is higher than usual values found in falling film absorbers using conventional circular tubes. Moreover, the new adiabatic configuration presented has significant advantages respect to the non-adiabatic one in terms of higher r_{qV} and fabrication simplicity.

* Corresponding author.
E-mail address: mvenegas@ing.uc3m.es (M. Venegas).

Keywords: Absorption refrigeration; adiabatic; absorber; membranes; rectangular microchannels; water–lithium bromide

Nomenclature

A	adiabatic absorber
A	area (m^2)
C_p	specific heat (kJ kg^{-1} K^{-1})
D_h	hydraulic diameter (m)
d_p	membrane pore diameter (m)
dz	discretisation length (m)
e	height or thickness (m)
h	convective heat transfer coefficient (W m^{-2} K^{-1})
i	specific enthalpy (kJ kg^{-1})
J	absorption rate (kg m^{-2} s^{-1})
k	thermal conductivity (W K^{-1} m^{-1})
$\tilde{k}$	mass transfer coefficient (m s^{-1})
K	mass transfer coefficient (kg m^{-2} s^{-1} Pa^{-1})
l	width (m)
L	total length of channels (m)
$\dot{m}$	mass flow rate (kg s^{-1})
NA	non-adiabatic absorber
Nu	Nusselt number, $Nu = hD_h/k$
P	pressure (Pa)
Pr	Prandtl number, $Pr = \mu C_p/k$
q	thermal power (W)
R	mass transfer resistance (kg^{-1} Pa m^2 s)
Re	Reynolds number, $Re = uD_h\rho/\mu$
r_{qV}	ratio between cooling capacity and absorber volume (W m^{-3})
T	temperature (ºC)
u	velocity (m s^{-1})
U	global heat transfer coefficient (W m^{-2} K^{-1})
V	volume (m^3)
w	centre-to-centre distance (m)

x lithium bromide mass fraction ($kg_{LiBr}\ kg_s^{-1}$)

z length (m)

z^* dimensionless length, $z^* = z/(RePrD_h)$

Greek symbols

α channel aspect ratio, $\alpha = l/e$.

ε porosity

μ viscosity (Pa s)

Ξ Ackermann factor

ρ density ($kg\ m^{-3}$)

Φ heat transfer rate factor

Subscripts

a absorber

A adiabatic absorber

cw cooling water

fd fully developed

l liquid

m membrane

NA non-adiabatic absorber

ov overall

s solution

sat saturation

th thermal

T total

v vapour

va vapour absorbed

w wall

1. Introduction

The absorber is one of the major size components of absorption cooling chillers and one of which most limits the performance. In order to increase the heat and mass

transfer in the solution, several configurations have been proposed for the liquid and vapour streams in the absorber. These include laminar and turbulent falling films, bubbly flows, use of atomizers to disperse the solution in droplets of different sizes or sheets, etc. Nevertheless, all of them present relatively low heat and mass transfer coefficients and lead to large, heavy and rigid heat exchangers. Cooling water from a cooling tower is conventionally used to extract the heat released during the absorption process.

Currently, new technologies are being evaluated. One of them uses microporous membranes at the interface between solution and vapour, and the solution is confined in rectangular microchannels. In the membrane, many pores of small diameter avoid mixing between vapour and solution, while allowing the vapour and solution to be in contact. Thanks to the surface tension effect, the solution doesn't enter into the pores and only the vapour diffuses through them. The difference between the vapour pressures at both sides of the membrane causes the mass transfer. If compared to conventional absorbers, advantages of using microporous membranes in combination with microchannels include a larger contact area between solution and vapour per unit volume, which allows a higher compactness. Also, the solution and vapour flow rates can be controlled independently and the absorber can be fabricated of different sizes with an easier scale up.

Previous studies about membrane-based absorbers using flat membranes in rectangular microchannels include theoretical and experimental works. Ali and Schwerdt [1, 2], developed theoretical studies using the H_2O-LiBr solution. They specified the characteristics of an appropriate membrane to be used in the absorber. A higher thickness of the membrane leads to higher mass transfer resistance, while the mechanical stability improves. As a compromise between both constraints, the authors concluded that the layer thickness should be up to 60 micron. In a later study, Ali and Schwerdt [3] concluded that a porosity value of 0.8 combined with a large pore diameter leads to an almost doubled water vapour flux through the membrane compared to a 0.5 porosity value. With the aim of achieving higher vapour fluxes, and taking into account the strength needed for the secure fixation of the membrane inside the absorber, the authors recommended that an appropriate membrane should have a porosity ranging between 0.7 and 0.8. Reducing the solution film thickness from 2.5 to 1.0 mm, Ali [4] obtained about a 20% higher absorption rate.

Using the same solution, a numerical investigation about the performance of a membrane-based absorber was developed by Yu et al. [5]. They showed that several folds enhancement in the absorption rate can be achieved with respect to conventional absorbers. Isfahani and Moghaddam [6] developed experiments using a superhydrophobic membrane of 1 micron pore size and 80% porosity, obtaining absorption rates of around 0.006 kg m^{-2} s^{-1}. In their tests, they used channels of 100 micron thickness, while the solution velocity was 5 mm s^{-1}. Maximum pressure drop obtained was about 3 kPa, with no evidence of deteriorating the absorber performance. Isfahani et al. [7] presented permeability studies of highly porous nanofibrous membranes, concluding that membranes with a pore size higher than about 1 micron are valid for their use in the absorber. In a next study, Isfahani et al. [8] used microstructures to manipulate the thermohydraulic characteristics of the H_2O-LiBr flow in a membrane-based absorber in order to enhance the absorption rate.

Schwerdt [9] developed a compact stack design with flat sheet membranes. He concluded that the drafted module design seems promising based on multiplication to achieve the nominal cooling capacity. Bigham et al. [10] developed a study including micro-scale features at the surface of the solution channels, showing an increase in the mass transport. A review about the use of membranes in absorbers of absorption cooling systems was performed by Asfand and Bourouis [11], while Asfand et al. [12] developed a CFD simulation of a membrane-based absorber. They concluded that the absorption rate increased by a factor of 2.5 when the solution inlet flow velocity was augmented from 1.18 to 4.72 mm s^{-1}.

Lately, Venegas et al. [13] developed a simple model of a miniaturized absorber using membrane technology. The model was validated using data of Isfahani and Moghaddam [6]. The heat and mass transfer model developed considers that temperature and/or concentration could change along both thermal entrance and fully developed flow regions. In [13], the effect on the absorber performance of the aspect ratio of the cooling water and solution channels was evaluated. Venegas et al. [14] developed a parametric study to evaluate the sensitivity of the ratio between the cooling capacity of the chiller and the absorber volume to changes in some operating and design parameters. It was concluded that, at the design stage, the most important parameters are pore diameter, porosity, membrane thickness and solution channels depth. For a good performance during operation of the absorber, special care should be taken to select the adequate solution concentration and temperature at the inlet and vapour pressure.

All of the previous studies considered the extraction of the absorption heat released by a cooling water flow. In the present work, a promising new technology is evaluated, consisting in the use of microporous membranes in adiabatic absorbers using rectangular microchannels. The configuration here proposed consists of one or several modules (depending on the cooling capacity of the chiller) that contain two vapour channels, separated from the solution by adjacent microporous membranes. The solution is confined in the rectangular microchannels. A plastic or synthetic wall separates the solution channels between them. The solution entering the absorber is previously subcooled in an external heat exchanger using ambient air as cooling fluid. In this way, the need for a cooling tower is avoided.

The knowledge of the processes related to the mass and heat transfer in adiabatic absorbers, using membrane technology in microchannel heat exchangers, is of great importance to achieve further reductions of size. In the present work, a comparison between the adiabatic (A) and the non-adiabatic (NA) membrane-based absorbers using the water-lithium bromide solution is performed with the aim of identifying the least volume configuration. A new model is developed now for the A-absorber, based on the previous model presented in Venegas et al. [13] for the NA-absorber. The final objective of the comparison is to minimize the absorber volume, in order to reduce the size of absorption cooling chillers. The variable used to characterise the absorber compactness is the ratio between the cooling power of the chiller and the absorber volume.

2. Modelling of the absorption process

The absorber configurations used in the current study are shown in Fig. 1 to Fig. 4. They are plate-and-frame membrane modules, with the geometrical data and operating variables described in Table 1. The modules contain two vapour channels, separated from the solution by adjacent microporous membranes. The solution is confined in rectangular microchannels. A metal wall separates the cooling water channels from the solution channels in the NA-absorber. In the case of the A-absorber, the cooling water channels are avoided. In the complete design (not shown in Fig. 2), the channels walls are held in place joining their ends to a support framework. Additionally, thin perforated

plates are located over (or below) each membrane, to keep the membrane attached to the channel walls. To simplify the problem, the following assumptions are made:

- The system operates under steady state conditions and the heat and mass transfer are one dimensional.
- The solution, refrigerant vapour and cooling water (in the NA-absorber) completely fill their respective channels. Absorption takes place instantaneously and no incondensable gases are present. The assumption about no incondensable gases is valid for closed absorbers in vacuum conditions. In real absorption chillers, non-condensable gas detectors and purge systems are used to remove these gases.
- The system is adiabatic with respect to its surroundings.
- An equilibrium state exists at the interface between vapour and solution.
- The solution equilibrium concentration is only a function of the solution temperature because pressure is considered constant along the channels.
- Cooling water, solution and vapour are well-mixed in each differential volume. Homogeneous concentration and temperature are considered in all the points within each control volume.

Base case data shown in Table 1 were selected taking into account the following criteria:

- Solution and cooling water channel height and width are the same values used in previous articles of the authors [13, 14]. These values provide the highest ratio between cooling power and absorber volume, as shown in [14] and also in the present study for the case of the solution channel dimensions.
- Solution concentration and temperature of solution and cooling water at the inlet are typical values used in single-effect H_2O-LiBr absorption chillers.
- Cooling water mass flow rate is equal to values used in previous articles of the authors [13, 14]. As shown in [14], this parameter has a negligible importance on the ratio between cooling power and absorber volume.
- Solution mass flow rate is selected equal to the cooling water flow rate. This value is additionally modified in a wide range in the parametric analysis performed in the current study.
- The membrane characteristics correspond to commercially available membranes, usable in absorbers with the H_2O-LiBr solution, with a low thickness to reduce mass transfer resistance, but sufficiently high to provide mechanical strength.

- Vapour mass flow rate at the inlet allows sufficient vapour is available to be absorbed by the solution in all the cases simulated. According to the parametric study presented in [14], this variable does not greatly influence the results. The dimensions of the vapour chamber allow distribution of the vapour over the whole membrane.
- The length of the channels corresponds approximately to the point where the A- and NA-absorber reach the same ratio between cooling power and absorber volume.
- The temperature and pressure of the vapour are those conventionally used in H_2O-LiBr absorption chillers for air-conditioning purposes.
- The metal wall thickness and the centre-to-centre distance of the solution and cooling water channels, are real values provided by a manufacturer.

2.1. Heat transfer

The energy rate balance applied to the differential element shown in Fig. 3, for the case of the NA-absorber, is written as:

$$(\dot{m}_{va} i_{lv})^j = q_s^j + q_v^j + q_{cw}^j \quad (1)$$

In the case of the A-absorber (Fig. 4), the energy rate balance can be written as:

$$(\dot{m}_{va} i_{lv})^j = q_s^j + q_v^j \quad (2)$$

Left term in Eqs. (1) and (2) includes the heat released during absorption by the solution of the vapour mass flow rate $\dot{m}_{va}$. Right terms are related to the heat transferred to the solution (q_s^j), vapour (q_v^j), and cooling water (q_{cw}^j). These heat transfer rates for parallel flow are calculated as follows:

$$q_s^j = (\dot{m} \cdot i)_s^{j+1} - (\dot{m} \cdot i)_s^j \quad (3)$$

$$q_v^j = (\dot{m} \cdot i)_v^{j+1} - (\dot{m} \cdot i)_v^j \quad (4)$$

$$q_{cw}^j = \dot{m}_{cw}\left(i_{cw}^{j+1} - i_{cw}^j\right) = \dot{m}_{cw} Cp_{cw}^j \left(T_{cw}^{j+1} - T_{cw}^j\right) \quad (5)$$

In the present model, part of the heat released during absorption is transferred from the solution to the cooling water and the vapour, in the case of the NA-absorber, and only to the vapour in the case of the A-absorber. The following relations apply:

$$q_{cw}^j = U_{s\_cw}^j A\left(T_s^j - T_{cw}^j\right) \quad (6)$$

$$q_v^j = U_{s\_v}^j A\left(T_s^j - T_v^j\right) \quad (7)$$

The global heat transfer coefficients in Eqs. (6) and (7) are calculated as:

$$\frac{1}{U^j_{s\_cw}} = \frac{1}{h^j_{cw}} + \frac{e_w}{k^j_w} + \frac{1}{h^j_{s,cw*}} \tag{8}$$

$$\frac{1}{U^j_{s\_v}} = \frac{1}{h^j_v} + \frac{e_m}{k^j_{m,ave}} + \frac{1}{h^j_{s,v*}} \tag{9}$$

The average value of the membrane thermal conductivity $k_{m,ave}$ is determined using the classical parallel model, as given in Martínez and Rodríguez-Maroto [15]:

$$k_{m,ave} = \varepsilon k_v + (1-\varepsilon) k_m \tag{10}$$

where k_v is the thermal conductivity of the refrigerant vapour within the pores and k_m is the one corresponding to the material that forms the membrane.

Convection heat transfer coefficients in Eqs. (8) and (9), along the different channels, are calculated taking into account the difference between the thermal entrance region and the fully developed flow. Correlations used were selected also considering the dimensions of the channels. Specifically, for the cooling water and solution channels, the correlations developed by Lee and Garimella [16] has been used. They allowed the assessment of the thermal entry length and the convective heat transfer coefficients in that zone. The last correlation, shown in Eq. (11), allows predicting the convection coefficient for each point along the channel. Further, it covers a wide aspect ratio range and many hydraulic diameters. The equations required for obtaining C_1 to C_4 and the dimensionless length of the thermal entry zone z^*_{th} can be consulted in Venegas et al. [13].

$$Nu_{th} = \frac{1}{C_1 (z^*)^{C_2} + C_3} + C_4, \qquad \text{for } 1 \le \alpha \le 10,\ z^* < z^*_{th} \tag{11}$$

In the region corresponding to fully developed flow, the correlation derived by Shah and London [17], shown in Eq. (12) and valid for rectangular channels, was used to estimate the convection coefficients along the cooling water and solution channels.

$$Nu_{fd} = 8.235 \left(1 - \frac{2.0421}{\alpha} + \frac{3.0853}{\alpha^2} - \frac{2.4765}{\alpha^3} + \frac{1.0578}{\alpha^4} - \frac{0.1861}{\alpha^5}\right) \tag{12}$$

As mass transfer affects the heat transfer process, its effect was taken into account in the case of the solution channel. Convection coefficients obtained from Eqs. (11) and (12) were modified by the Ackermann factor (Taylor and Krishna [18]):

$$\Xi = \frac{\Phi}{e^{\Phi} - 1} \tag{13}$$

where the heat transfer rate factor Φ is defined as:

$$\Phi = J \cdot Cp_v \cdot e_s / k_v \tag{14}$$

When the heat transfer occurs in the same direction of mass transfer, the convection coefficient is incremented. If both processes are reverse, the heat transfer coefficient is

reduced. The first case corresponds to the heat transfer from the solution channel to the cooling water and the second one to the vapour.

In the case of the vapour channel, it is a rectangular channel with $D_{h,v} = 8$ mm and $\alpha_v = 4$. In this case, the Nusselt number in the developing region, the dimensionless thermal entry length and the Nusselt number in the thermally developed flow have been calculated using the correlations derived by Venegas et al. [13]. Correlations for the developing and fully developed regions are, respectively:

$$Nu_{th,v} = -3 \cdot 10^{-5}(z_v^*)^2 + 0.0307 z_v^* + 5.2901 \quad (15)$$

$$Nu_{fd,v} = -\frac{0.037}{\alpha_v^2} + \frac{0.7639}{\alpha_v} + 2.8036 \quad (16)$$

2.2. Mass transfer

Mass rate balances for the solution, water vapour and salt give the mass flow rates and LiBr mass fraction in the differential element *j*+1. The vapour mass flux through the membrane is calculated taking into account the conditions in the solution and water vapour streams. For the differential element *j*, the mass flow rate of vapour absorbed ($\dot{m}_{va}$) depends on the transfer area (A) and the absorption rate (J):

$$\dot{m}_{va}^j = J^j \cdot A \quad (17)$$

where:

$$A_{\mathrm{NA}} = l_s \cdot dz \quad (18)$$

$$A_{\mathrm{A}} = 2 \cdot l_s \cdot dz \quad (19)$$

$$J^j = \left(P_v - P_s^j\right)/R_{ov}^j \quad (20)$$

P_v and P_s in Eq. (20) are, respectively, the pressure in the vapour channel and the partial pressure of the water vapour, calculated at the solution temperature (T_s) and concentration (x). The overall mass transfer resistance between water vapour and solution (R_{ov}) includes the resistance to diffusion through the solution boundary layer (R_s) and the resistance to diffusion of water vapour through the membrane (R_m). Both resistances are in series:

$$R_{ov}^j = \frac{1}{K_{ov}^j} = R_s^j + R_m^j \quad (21)$$

Depending on the value of the ratio between the molecule mean free path and the pore diameter (Knudsen number), different mechanisms for vapour transport through the membrane exist: Knudsen diffusion, transition flow and viscous flux (Poiseuille

flow). For each of these regimes, the transport resistance can be calculated in different ways, as described in Venegas et al. [14]. For the conditions given in Table 1 and the parametric study performed in the present work, Knudsen number ranges between 13.28 and 14.18. Consequently, free molecular flow occurs through the membrane along the absorber.

Mass transfer resistance within the solution (R_s) is estimated as in Ali and Schwerdt [2]:

$$R_s^j = \frac{P_{sat}^j}{\rho_{water}^j \tilde{k}_s^j} \tag{22}$$

In Eq. (22), P_{sat} is the pressure of the saturated water at the temperature of the solution, ρ_{water} is the density of the liquid water and $\tilde{k}_s$ is the mass transfer coefficient between the bulk solution and the vapour-solution interface. In this work, $\tilde{k}_s$ is estimated using analogy between heat and mass transfer, as in Venegas et al. [13]. For the thermal entrance region, correlation of Lee and Garimella [16] has been used, while for fully developed flow the one of Shah and London [17] has been selected.

The temperatures and concentration along the channels cannot be explicitly calculated from Eqs. (1) to (22). For this reason, the above set of equations was implemented in a computer code using Engineering Equation Solver software, EES™ [19]. Metal of the wall interface was considered AISI 316. Thermodynamic properties of the water-lithium bromide solution, water vapour and AISI 316 have been calculated using EES™. PTFE is selected as material for the membranes and its thermal conductivity is calculated using the correlation of Sperati et al. [20]. The diffusion coefficient of water in the water-lithium bromide solution has been calculated using the equation described by Mittermaier et al. [21].

Validation of the model for the NA-absorber was developed by comparison of the absorption rate predicted by the model with the test data offered by Isfahani and Moghaddam [6]. In their experiments, the cooling water and solution channels measured, respectively, 4 and 1 mm in width. The cooling water channel height was 0.4 mm, while two depths were used for the solution channels, 0.1 and 0.16 mm. All the correlations used in the model remain valid in all the cases evaluated in the present study. The mean absolute error of the model predictions respect to the experimental data shown in Venegas et al. [13] is 8.5%.

3. Results and discussion

In the following sections, results obtained from the simulation show, in Figs. 5 to 9, the evolution along the solution channels of the pressure potential (P_v-P_s), solution concentration (x), absorption rate (J), overall mass transfer coefficient (K_{ov}), solution temperature (T_s), heat exchanged/stored in the working fluids (q_{cw}, q_s), cooling power of the chiller ($q_{chiller}$) and the ratio between the cooling power and the absorber volume (r_{qV}):

$$r_{qV} = {}^{q_{chiller}}/_{V_a} \tag{23}$$

In the last section, a parametric analysis is performed to evaluate the influence on the A- and NA-absorber performance of the solution temperature (T_s) and mass flow rate ($\dot{m}_{s,T}$) at the inlet of the channels, and of the solution channel height (e_s) and width (l_s). Results are presented in Figs. 10 to 13.

All the data considered for the simulation are those given in Table 1, except when specified.

3.1. Evolution along the channels

In Fig. 5 the variation of the pressure potential is represented as a function of the channel length. As expected, a higher pressure potential is reached in the NA-absorber, because the solution is continuously subcooled. This subcooling reduces the equilibrium pressure P_s, corresponding to the given temperature and concentration. The pressure potential continuously decreases in the A-absorber because the solution increases its temperature continually due to the absorption heat release. The pressure potential influences the absorption process as represented by Eq. (20).

Fig. 6 shows the evolution of the absorption rate and the overall mass transfer coefficient in both absorbers. Both parameters are higher in the NA-absorber because the absorption heat is extracted by the cooling water and the solution is continuously cooled. The values obtained tend to decrease as the solution absorbs the vapour along the channels, and the subcooling of the solution decreases. Average absorption rates of $2.3 \cdot 10^{-3}$ and $3.3 \cdot 10^{-3}$ kg m^{-2} s^{-1} are obtained in the A-absorber and NA-absorber respectively.

The variation of the solution and cooling water temperatures along the absorption channels is shown in Fig. 7. A slight variation of the solution temperature is observed in the case of the NA-absorber due to heat transfer to cooling water. Firstly, as the cooling

water temperature is sufficiently low, the solution is cooled. Secondly, the solution temperature increases as absorption progresses and the cooling water temperature augments. The cooling water temperature continuously increases governed by the absorption heat release, analogous to the solution temperature increase in the case of the A-absorber. The variation of the solution temperature observed in this figure directly relates to the performance observed in the pressure potential represented in Fig. 5. It implies that, the lower the solution temperature is, the higher the potential for mass transfer will be.

Fig. 8 represents the evolution of the thermal power stored in the solution and transferred to the cooling water per unit length of the absorption channels. In the case of the A-absorber, the heat stored in the solution decreases very rapidly in the first part of the channel as the solution heats and the absorption rate decreases. The cooling water used in the NA-absorber initially heats as a result of the heat released during absorption and also due to the heat extracted from the solution. During around the first half of the channel length, the solution in the NA-absorber decreases its temperature releasing heat to the cooling water. From this point, solution begins storing heat. The evolution observed corresponds to the variation of the solution temperature shown in Fig. 7. The contribution of the power transferred to the vapour is not shown in Fig. 8 because it is almost two orders of magnitude smaller in both configurations.

The cooling power of an absorption chiller equipped with the absorbers modelled in the present work is represented in Fig. 9 as a function of the channels length for each type of absorber. This is the integrated cooling power obtained for the different lengths shown. Also, the ratio between this cooling power and the absorber volume (r_{qV}) is represented, supposing that the rest of chiller components perform similarly in both absorber configurations. As observed, this ratio suddenly increases with the channel length, reaching its maximum value (1505 and 1061 kW m^{-3} for the A- and NA-absorber respectively) at 2 mm length approximately. From this length, the ratio slowly decreases in the case of the NA-absorber until reaching the same ratio of the A-absorber at around 3 cm length (data in Table 1). From this point, r_{qV} is lower in the case of the A-absorber.

The increasing r_{qV} observed at the channel entrance is associated to the growing cooling power obtained, given the high absorption rate reached in this region as shown in Fig. 6. As this rate decreases when the channel length increases, the cooling power rises at a lower rate. This effect, combined with the enlargement of the absorber volume when the channel length increases, yields the maximum value for r_{qV} observed in Fig. 9. From this point, the fast decrease observed in r_{qV} for the A-absorber is associated to the solution

heating, which reduces its ability to absorb refrigerant vapour. This information about r_{qV} can be used to optimize the absorber size. Hence, when designing the absorbers it is not recommended to use very long channels, especially in the case of the A-absorber, because the increase of the absorber size is higher than the increment obtained in the cooling power.

The values of r_{qV} obtained in this work are higher than the ones found in horizontal falling film absorbers using the same solution, as modelled by Jeong and Garimella [22]. In that study, the ratio reaches a maximum value of 450.7 kW m^{-3} for conventional tubes of 15.88 mm diameter.

The main improvement of an absorption chiller if it incorporates a membrane-based absorber is its reduction in size respect to the use of conventional falling film absorbers. Additionally, the use of microchannels reduces the approach temperatures between the outlet solution and the inlet cooling water in the case of the NA-absorber. Consequently, using the same cooling water, the absorption rate increases as it is directly related to the subcooling of the solution. A higher absorption rate conducts to a more diluted solution at the outlet of the absorber, increasing the mass flow rate of refrigerant circulating through the evaporator, which improves the cycle performance.

3.2. Parametric analysis

Figs. 10 to 13 show, through a comparative study between the A- and the NA-absorber, the sensitivity of r_{qV} to the different parameters analysed in the present study. In all the figures, results represented correspond to r_{qV} at the end of the solution channel. Fig. 10 shows the influence of the inlet solution mass flow rate on r_{qV}. The simulated flow rates are the same in each solution channel, allowing the same inlet velocity in the A- and NA-absorber. A fast increment of r_{qV} is observed in Fig. 10 for both absorber configurations when the solution flow rate increases up to around 1 g s^{-1}. From this value, the increment of the solution mass flow rate yields to a continuous increase of r_{qV} (but at a lower speed) in the case of the A-absorber and it remains almost constant in the NA-absorber.

When the total solution flow rate is increased in the NA-absorber from 0.05 to 5 g s^{-1}, r_{qV} increases from 421 to 1143 kW m^{-3}. However, in the case of the A-absorber the same change in the inlet solution flow rate produces a higher increase in the ratio r_{qV}, from 205 to 1584 kW m^{-3}. A very positive effect is observed in the case of the A-absorber, because more solution is available to absorb the refrigerant vapour, increasing much less its

temperature, which improves the pressure potential. For this reason, the A-absorber configuration is specially recommended for high inlet solution flow rates.

Inlet temperatures of the working fluids are important parameters in the performance of absorbers. Fig. 11 shows that the solution inlet temperature has a strong linear effect on the absorber compactness. When it is reduced from 45 ºC to 25 ºC, the cooling power of the chiller equipped with an A-absorber of 1 m^3 volume increases from 119 to 1263 kW, i.e., approximately 57 kW K^{-1}. In the case of the NA-absorber, the cooling power increases from 443 to 1061 kW. As observed from these data, the influence of the solution inlet temperature is higher in the case of the A-absorber, because no heat extraction is produced along the absorption channels. In the case of the NA-absorber the solution temperature is continuously modified by heat transfer to the cooling water, resulting the inlet temperature effect on r_{qV} lower. For the base case of cooling water inlet temperature shown in Table 1 (25 ºC), solution inlet temperatures lower than 32 ºC are required in the A-absorber to reach higher r_{qV} than in the NA-absorber. This temperature increases if the cooling water inlet temperature increases, as shown in Fig. 11. For example, it reaches 35 ºC for a cooling water inlet temperature of 29 ºC.

The influence of the solution channel height and width is analysed independently in Figs. 12 and 13. In both figures, better r_{qV} values are obtained in the case of the A-absorber due to its lower volume. Differences between A- and NA-absorber increase when the solution channel height and width increases and reduces respectively. Respect to the absorber volume, also represented in Fig. 12, the size of the A-absorber changes slightly more than the corresponding variation of the NA-absorber, because only one row of solution channels is used in the first case (see Figs. 1 and 2). A small depth channel provides a small solution thickness, which reduces the solution mass transfer resistance and allows cooling a higher fraction of solution volume in the case of the NA-absorber. In the case of the A-absorber, when the solution channel height is reduced from 1.5 to 0.15 mm, the ratio r_{qV} increases from 347 to 869 kW m^{-3}. A similar effect on improving r_{qV} is obtained when the solution channel width is increased from 0.1 to 1.5 mm. In this case the ratio r_{qV} increases in the A-absorber from 526 to 869 kW m^{-3}. Very slight increases in r_{qV} are produced in both A- and NA-absorber when the solution channel width increases over around 0.3 mm.

4. Conclusions

A simulation of the heat and mass transfer processes taking place in membrane-based miniaturized A- and NA-adiabatic absorbers has been developed. Results presented show the variation along the channels of: absorption potential, solution concentration, absorption rate, overall mass transfer coefficient, solution and cooling water temperatures, thermal power transferred to cooling water and stored in the solution, cooling power and the ratio between the cooling power and the absorber volume. The effect of the solution inlet temperature, inlet solution mass flow rate and solution channels width and height is comparatively evaluated. The following conclusions have been drawn:

- The simulated absorbers have values of the ratio between cooling capacity of the chiller and absorber volume of around 1 MW m^{-3}, for the base case considered. These values are higher than the ones obtained using falling film absorbers of conventional-diameter tubes.
- In order to minimize the absorber volume for a given cooling power (maximize r_{qV}), the design of membrane-based absorbers should focus on short channels. Far from a very small channel length, any increase in the channel length tends to increase the absorber size higher than the increment obtained in the cooling power, especially in the case of the A-absorber.
- The A-absorber is very sensitive to the solution inlet temperature and inlet solution mass flow rate, as compared to the NA-absorber, because no heat extraction is produced along the channels. For the base case considered in this study, the A-absorber allows obtaining higher ratio between cooling capacity of the chiller and absorber volume for inlet solution flow rates higher than 0.5 g s^{-1} and solution inlet temperature lower than 32 ºC.

The promising new technology here proposed, using membrane contactors in adiabatic microchannel absorbers, can be used to reduce the weight and size of the absorbers, as they can be fabricated using plastic or synthetic materials and no cooling water channels are required. Because the solution can be previously subcooled using ambient air, the need for a cooling tower is avoided.

Acknowledgements

The financial support of this study by the Ministerio de Economía y Competitividad of Spain through the research grant ENE2013-43131-R is greatly appreciated.

References

[1] Ali AHH, Schwerdt P. Characteristics of the membrane utilized in a compact absorber for lithium bromide–water absorption chillers, Proc 9th Int IEA Heat Pump Conf, 2008, Switzerland, Paper ID 5.51.

[2] Ali AHH, Schwerdt P. Characteristics of the membrane utilized in a compact absorber for lithium bromide-water absorption chillers. Int J Refrig 2009;32:1886–96.

[3] Ali AHH, Schwerdt P. For designing a compact absorber with membrane contactor at liquid-vapor interface: influence of membrane properties on water vapour transfer. ASHRAE Trans 2010;116:398–407.

[4] Ali AHH. Design of a compact absorber with a hydrophobic membrane contactor at the liquid–vapor interface for lithium bromide–water absorption chillers. Appl Energy 2010;87:1112–21.

[5] Yu D, Chung J, Moghaddam S. Parametric study of water vapour absorption into a constrained thin film of lithium bromide solution. Int J Heat Mass Transf 2012;55:5687–95.

[6] Isfahani RN, Moghaddam S. Absorption characteristics of lithium bromide (LiBr) solution constrained by superhydrophobic nanofibrous structures. Int J Heat Mass Transf 2013;63:82–90.

[7] Isfahani RN, Sampath K, Moghaddam S. Nanofibrous membrane-based absorption refrigeration system. Int J Refrig 2013;36:2297–307.

[8] Isfahani RN, Bigham S, Mortazavi M, Wei X, Moghaddam S. Impact of micromixing on performance of a membrane-based absorber. Energy 2015;90:997–1004.

[9] Schwerdt P. Activities in thermal driven cooling at Fraunhofer Umsicht. In: Thermally driven heat pumps for heating and cooling. Ed. Annett Kühn. Universitätsverlag der TU Berlin, 2013:117–26.

[10] Bigham S, Yu D, Chugh D, Moghaddam S. Moving beyond the limits of mass transport in liquid absorbent microfilms through the implementation of surface-induced vortices. Energy 2014;65:621–30.

[11] Asfand F, Bourouis M. A review of membrane contactors applied in absorption refrigeration systems. Renew Sust Energ Rev 2015;45:173–91.

[12] Asfand F, Stiriba Y, Bourouis M. CFD simulation to investigate heat and mass transfer processes in a membrane-based absorber for water-LiBr absorption cooling systems. Energy 2015;91:517–30.

[13] Venegas M, de Vega M, García-Hernando N, Ruiz-Rivas U. A simple model to predict the performance of H2O-LiBr absorber operating with a microporous membrane. Energy 2016;96:383–93.

[14] Venegas M, de Vega M, García-Hernando N. Parametric study of operating and design variables on the performance of a membrane-based absorber, Appl Therm Eng 2016;98:409–19.

[15] Martínez L, Rodríguez-Maroto JM. Characterization of membrane distillation modules and analysis of mass flux enhancement by channel spacers. J Membr Sci 2006;274:123–37.

[16] Lee P-S, Garimella SV. Thermally developing flow and heat transfer in rectangular microchannels of different aspect ratios. Int J Heat Mass Transf 2006;49:3060–7.

[17] Shah RK, London AL. Laminar flow forced convection in ducts, In: A source book for compact heat exchanger analytical data. Advances in heat transfer, Suppl. 1. Academic Press, NewYork, 1978.

[18] Taylor R, Krishna R. Multicomponent mass transfer. John Wiley & Sons, New York, 1993.

[19] Klein SA. Engineering Equation Solver. Academic Professional, 1992-2016, V10.091-3D, 2016.

[20] Sperati CA, DuPont de Nemours EI. In: Polymer handbook, J. Brandrup, E.H. Immergut, editors. 3rd ed., John Wiley, New York, 1989.

[21] Mittermaier M, Schulze P, Ziegler F. A numerical model for combined heat and mass transfer in a laminar liquid falling film with simplified hydrodynamics. Int J Heat Mass Transf 2014;70:990–1002.

[22] Jeong S, Garimella S. Optimal design of compact horizontal tube LiBr/water absorbers. HVAC&R Research 2005;11:27–44.

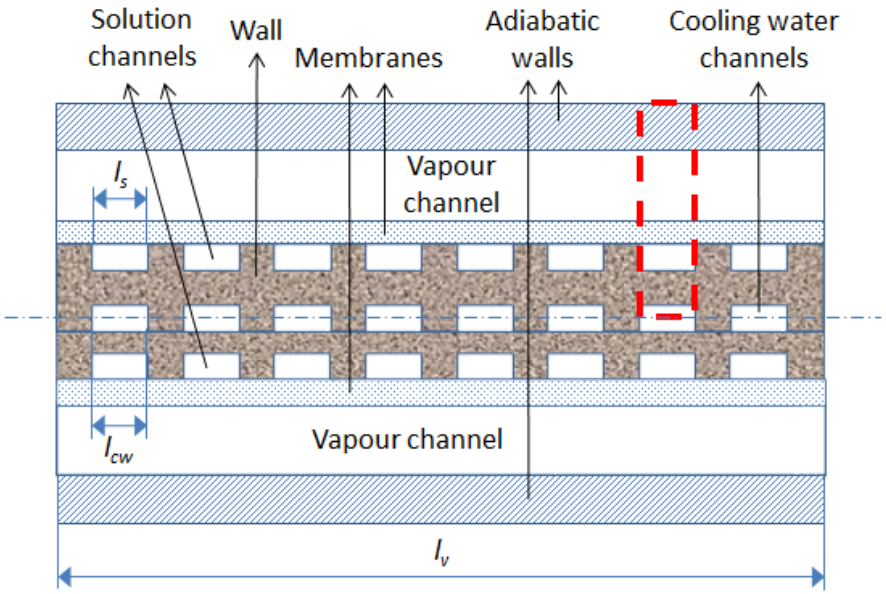

Fig. 1. Cross section of the non-adiabatic absorber.

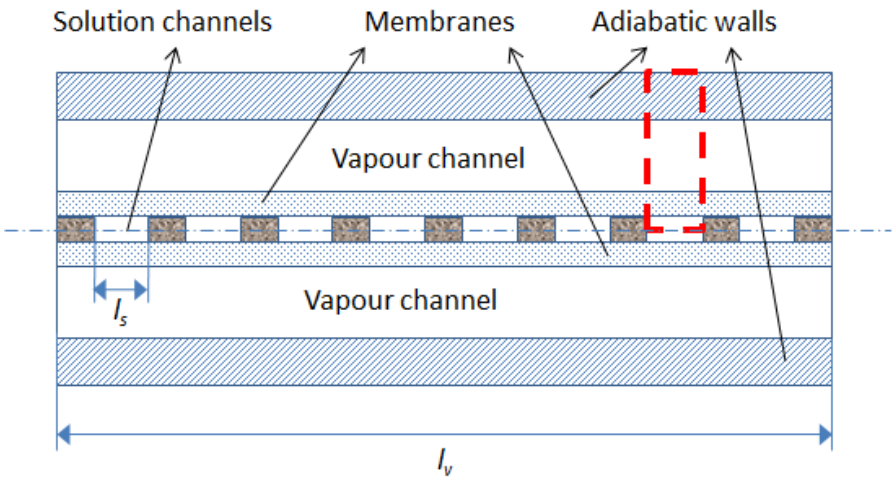

Fig. 2. Cross section of the adiabatic absorber.

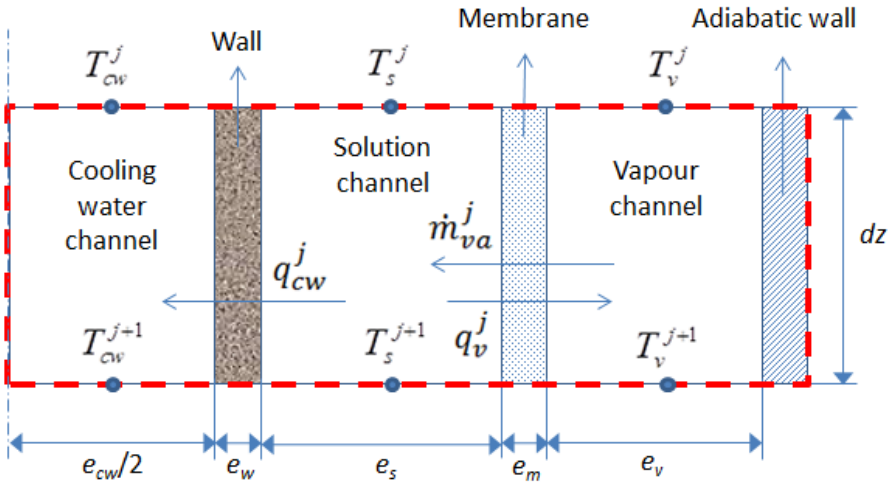

Fig. 3. Differential element of the non-adiabatic absorber.

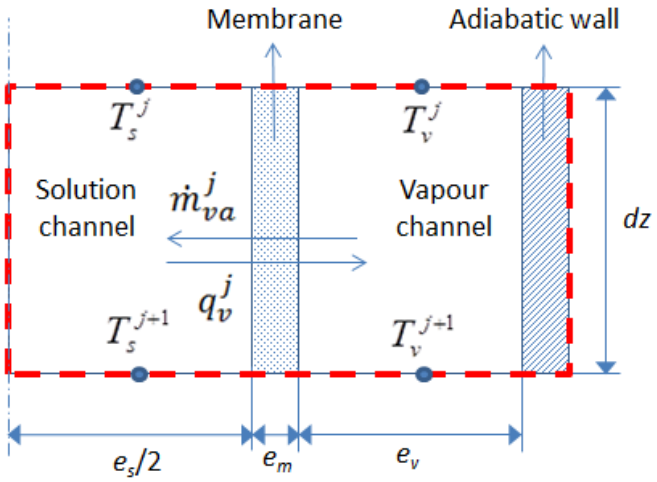

Fig. 4. Differential element of the adiabatic absorber.

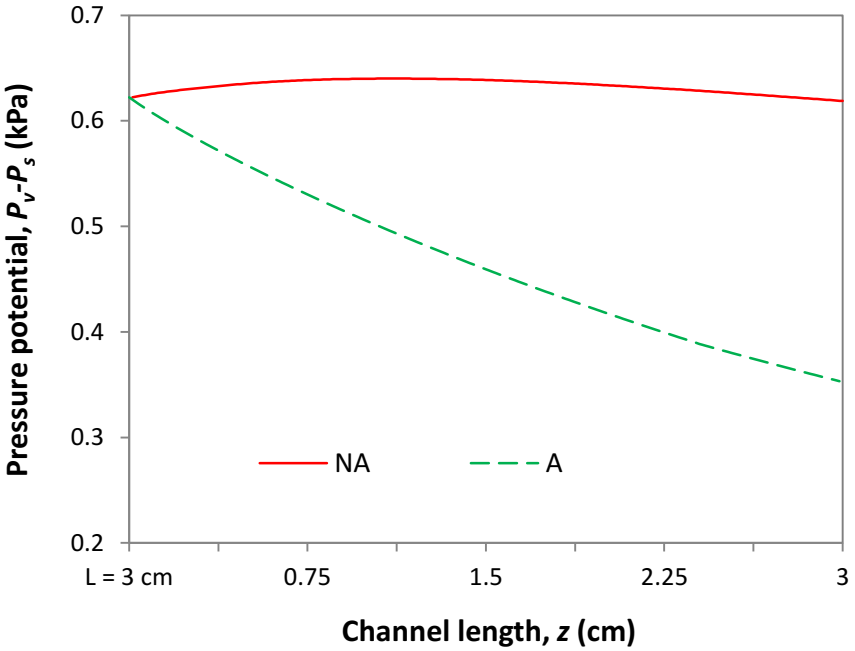

Fig. 5. Evolution along the absorption channels of the pressure potential.

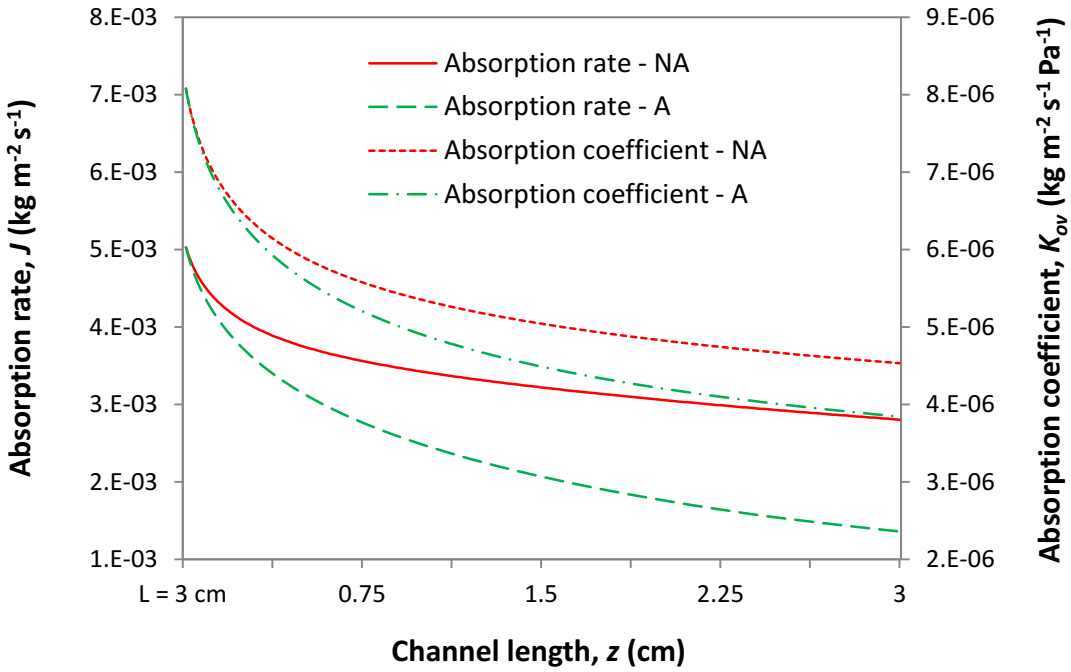

Fig. 6. Evolution along the absorption channels of the absorption rate and overall absorption coefficient.

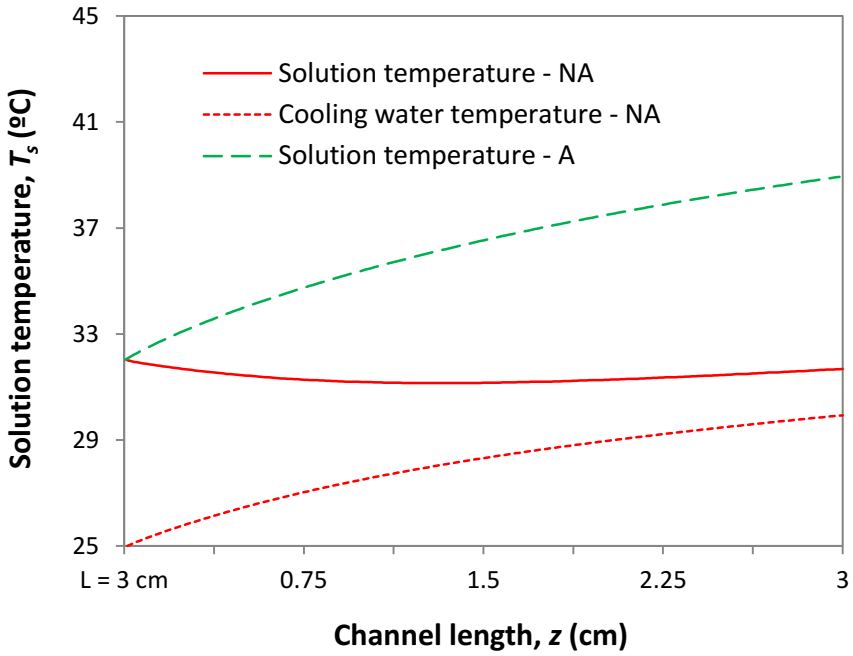

Fig. 7. Evolution along the absorption channels of the solution and cooling water temperatures.

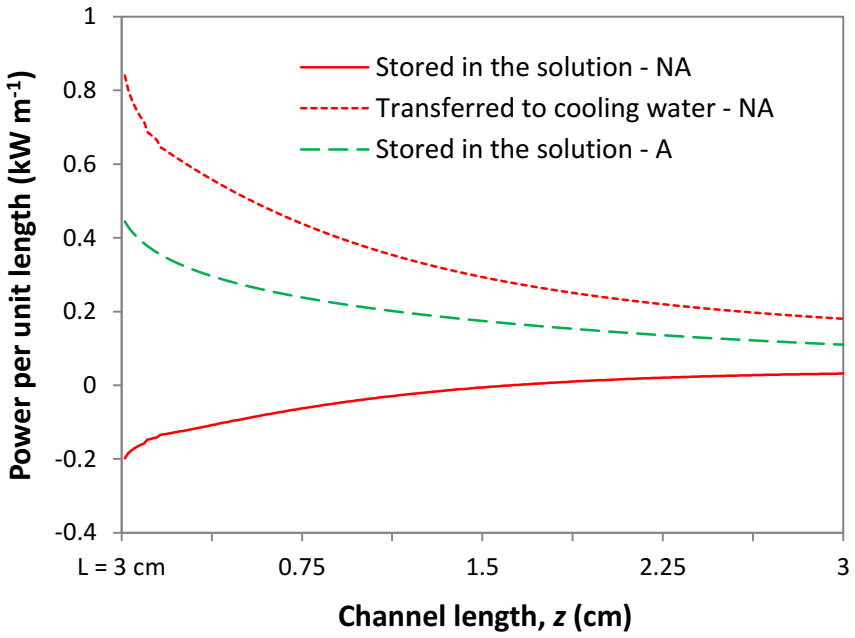

Fig. 8. Evolution along the absorption channels of the thermal power transferred to cooling water and stored in the solution.

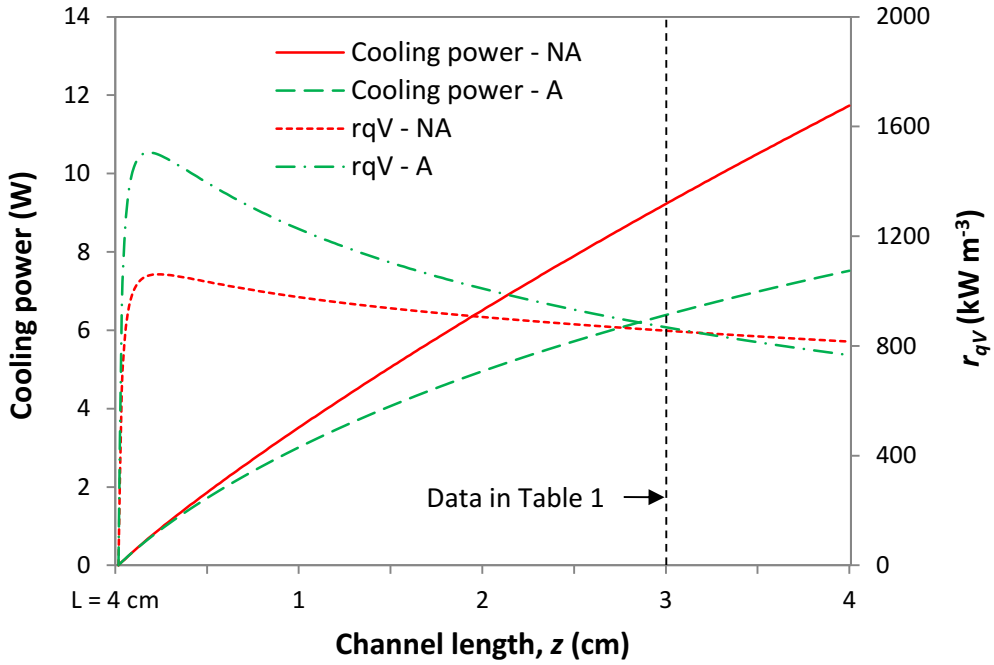

Fig. 9. Evolution of the cooling power and the ratio between the cooling power and the absorber volume (r_{qV}) along the absorption channels.

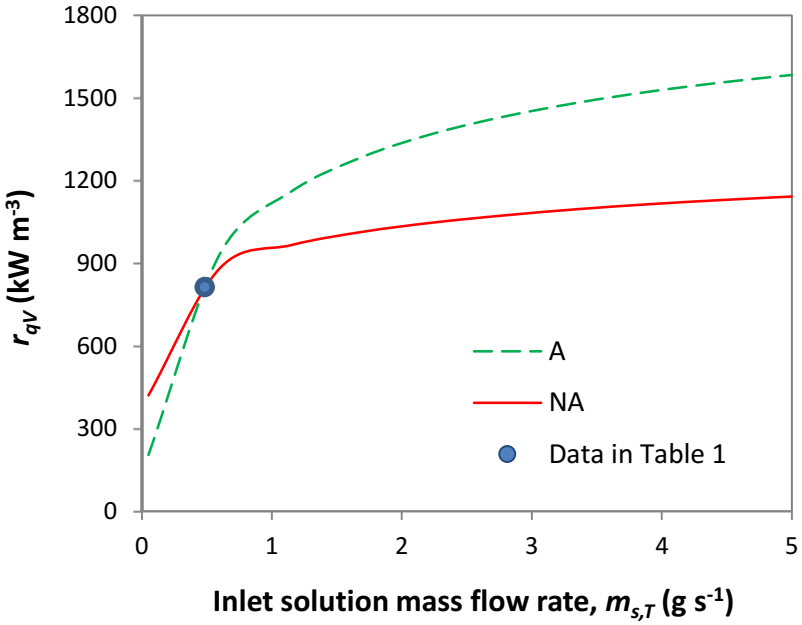

Fig. 10. r_{qV} for different inlet solution mass flow rate ($m_{s,T}$).

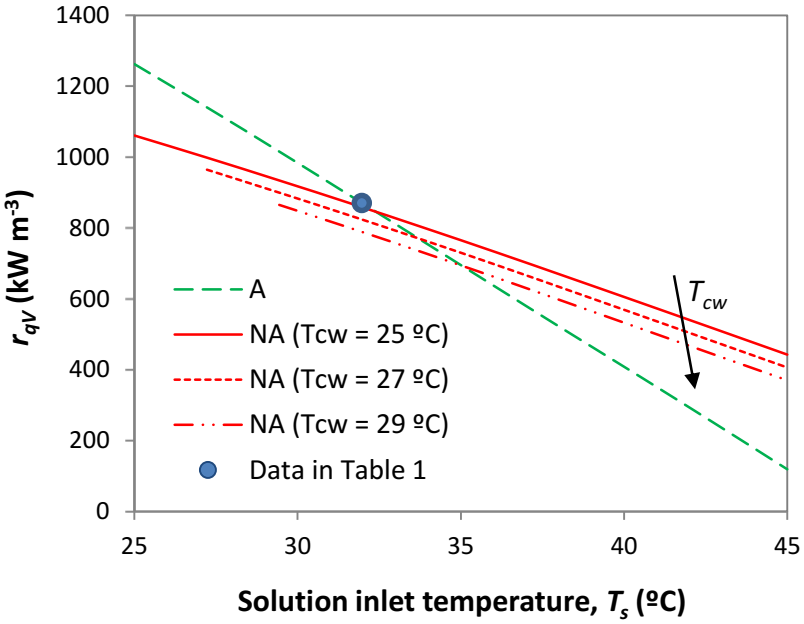

Fig. 11. r_{qV} for different solution inlet temperature (T_s).

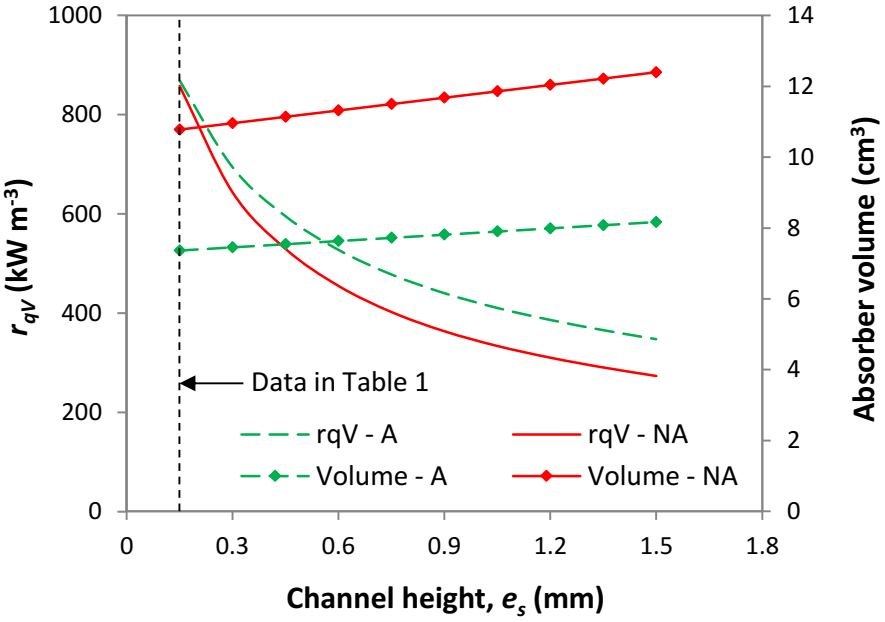

Fig. 12. r_{qV} for different solution channels height (e_s).

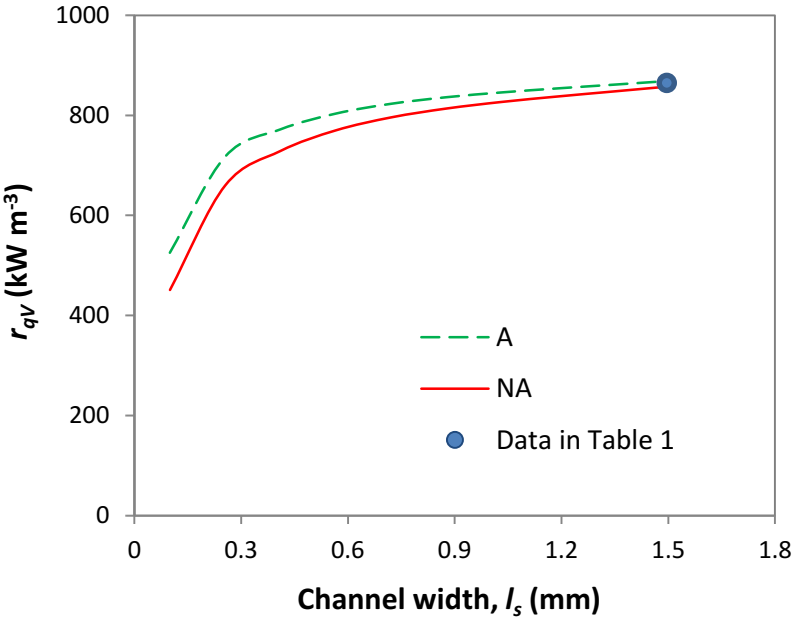

Fig. 13. r_{qV} for different solution channels width (l_s).

Table 1. Base case data considered for the simulation, corresponding to the schemes of the absorber represented in Figs. 1 to 4.

Parameter	Value
Vapour pressure, P_v (kPa)	1
Metal wall thickness, e_w (mm)	2.7
Membrane thickness, e_m (μm)	60
Vapour channel height, e_v (mm)	5
Solution channel width, l_s (mm)	1.5
Vapour channel width, l_v (mm)	20
Discretization length, dz (mm)	0.13
LiBr mass fraction at the inlet, x	0.6
Centre-to-centre distance of the solution and cooling water channels, w_s, w_{cw} (mm)	1.6
Length of channels, L (cm)	3
Cooling water inlet temperature, T_{cw} (ºC)	25
Solution inlet temperature, T_s (ºC)	32
Vapour inlet temperature, T_v (ºC)	7
Cooling water channel width, l_{cw} (mm)	1.5
Solution channel height, e_s (mm)	0.15
Cooling water channel height, e_{cw} (mm)	0.15
Vapour mass flow rate at the inlet, $\dot{m}_v$ (mg s^{-1})	40
Membrane porosity (%)	80
Membrane pore diameter, d_p (μm)	1
Total cooling water and solution mass flow rates at the inlet, $\dot{m}_{cw,T}$, $\dot{m}_{s,T}$ (g s^{-1})	0.5